INTERNATIONAL JOURNAL FOR NUMERICAL METHODS IN ENGINEERING
Int. J. Numer. Meth. Engng 2012; **92**:507–530
Published online 27 June 2012 in Wiley Online Library (wileyonlinelibrary.com). DOI: 10.1002/nme.4344

Improving multiresolution topology optimization via multiple discretizations

Tam H. Nguyen, Glaucio H. Paulino*,†, Junho Song and Chau H. Le

Department of Civil and Environmental Engineering, University of Illinois, Urbana, IL 61801, USA

SUMMARY

Unlike the traditional topology optimization approach that uses the same discretization for finite element analysis and design optimization, this paper proposes a framework for improving multiresolution topology optimization (iMTOP) via multiple distinct discretizations for: (1) finite elements; (2) design variables; and (3) density. This approach leads to high fidelity resolution with a relatively low computational cost. In addition, an adaptive multiresolution topology optimization (AMTOP) procedure is introduced, which consists of selective adjustment and refinement of design variable and density fields. Various two-dimensional and three-dimensional numerical examples demonstrate that the proposed schemes can significantly reduce computational cost in comparison to the existing element-based approach. Copyright © 2012 John Wiley & Sons, Ltd.

Received 19 January 2010; Revised 20 September 2011; Accepted 2 April 2012

KEY WORDS: density mesh; design variable; multiresolution; adaptive optimization; finite elements; multiresolution topology optimization (MTOP)

1. INTRODUCTION

Structural topology optimization has been successfully applied to a variety of practical engineering problems in the past decades [1, 2]. However, challenges still remain in enhancing computational efficiency despite the rapid improvement in computer performance. This is because the requirement of high fidelity is also increasing constantly, especially for three-dimensional (3D) applications. In general, computational cost depends on those of the analysis and the optimization process. This study aims to develop an approach to reduce the computational cost in both the analysis and the optimization while maintaining high resolution designs. Our development includes two parts: reducing the number of design variables and adaptively improving multiresolution topology optimization by using appropriate elements at suitable locations.

In general, the topology optimization method seeks an optimal distribution of material in the design domain to optimize the performance of a structure under given constraints. In the material distribution method, topology of a structure is defined through the density of pixels/voxels in the domain [3]. The density can be considered as a design variable and can assume an intermediate value between 0 (void) and 1 (solid). To obtain a well-defined solution, a relatively large number of finite elements and design variables are often required, which naturally makes the problem computationally expensive or intractable. Studies devoted to developing efficient approaches for large-scale topology optimization problems have been focused on the solution of finite element analysis because of its dominance in the computational cost [4, 5]. These approaches [4–13] can be broadly divided into three groups: (1) employing powerful computing resources; (2) introducing efficient solution

*Correspondence to: Glaucio H. Paulino, Department of Civil and Environmental Engineering, University of Illinois at Urbana-Champaign, Newmark Laboratory, 205 North Mathews Avenue, Urbana, IL 61801, U.S.A.

†E-mail: paulino@illinois.edu

for the analysis; and (3) reducing the number of degrees of freedom of the analysis model. In the first approach, parallel computing is often used to handle a large number of finite elements [5–8]. In the second approach, fast iterative solvers are developed to handle large-scale three-dimensional finite element analysis [4, 7–9]. Additionally, in reanalysis procedures [10], finite element analyses are performed only at an interval of several iterations, while the displacements are approximated at other iterations. Thus, the total number of finite element analyses is reduced in comparison to the full analysis at every optimization iteration. In the third approach, multiple mesh size strategies [11–13] have been studied to reduce the computational cost by solving the problem first on a coarse mesh and later on a refined mesh during the topology optimization process. The above-mentioned studies employ the same discretization for the finite elements and design variables.

There have been some studies to decouple the models used for analysis and design optimization. Traditional topology optimization methods, such as the element-based approach, utilize the density of each finite element as a design variable. The design variables can be located at the centers, at the nodes, or at the midpoints of the edges of the finite elements [14–17]. The topology definition function is also utilized to decouple the topology definition and the finite element analysis [18]. The super-element approach [19] represents the densities of several finite elements by a single design variable. The aforementioned decoupling approaches utilize two meshes: the finite element (FE) mesh, and the design variable mesh. In these approaches, the design variable mesh is similar or coarser than the finite element mesh. A multiresolution topology optimization (MTOP) approach [20] has been recently proposed using three meshes (not necessarily uncorrelated): the finite element mesh for the analysis, the design variable mesh for the optimization, and the density element mesh for material distribution representation. In this approach, the design variable and density element meshes are finer than the finite element mesh. The governing equation is solved on the coarser finite element mesh while the optimization is performed on the finer design variable mesh. In Reference [20], the design variable mesh and the density mesh are the same. Because the computational cost for solving the governing equation is dominant in a problem using traditional topology optimization approaches (e.g., element-based approach) [4,5], this approach can deal with large-scale problems at a relatively low computational cost [20]. The approach can promote high-resolution topology optimization in various problems including biomedical problems such as optimal design of craniofacial segmental bone replacements [21], and reliability-based topology optimization [22, 23].

In the first part of this paper, we propose an efficient scheme for improving multiresolution topology optimization (iMTOP) by using multiple distinct discretizations: a relatively coarse mesh for finite elements, a moderately fine mesh for design variables, and a relatively fine mesh for density elements as shown in Figure 1. Compared with our previous study in [20], the present work further reduces the computational cost while maintaining the resolution by using a coarser mesh for design variables. In topology optimization, one is usually motivated to refine the finite element mesh to obtain topology with smooth material boundaries. This is desirable especially for three-dimensional structures. For instance, after the optimal topology is obtained, the solution can be interpreted by using isosurfaces to define the contour of the solid part of the structure, which can be verified by means of finite element analyses. If the original mesh is coarse, a jagged isosurface may be obtained, which may require mesh repair and smoothening before it can be used for volume mesh generation. To a certain extent, we achieve this desirable effect (smooth boundaries) with our algorithm without having to refine the finite element mesh.

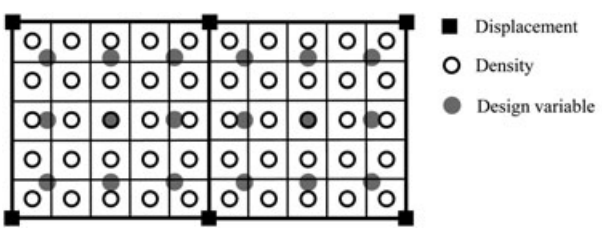

Figure 1. Displacement, density and design variable meshes.

DOI: 10.1002/nme

In the second part of this paper, we propose an adaptive multiresolution topology optimization (AMTOP) scheme to further increase the efficiency. The adaptive mesh refinement approach [24–26] has been proposed to reduce the total number of finite elements by representing the void with fewer (coarser) elements and the solid with more (finer) elements. Lin and Chou [11] proposed a two-stage approach in which the first-stage is performed with coarse finite elements and the optimal topology at the end of the first stage is used as the starting point for the second stage, which uses a fine FE mesh. In another investigation, Costa and Alves [24] employed a sequence of optimizations and mesh refinement, and used a converged solution on a coarse mesh to guide the refinement on the next refined mesh. Additionally, Stainko [25] used a slightly different approach in which the mesh is refined only on the material boundary. Recently, de Sturler *et al*. [26] refined the mesh in the solid regions and coarsened the mesh in the void regions dynamically, that is, during the optimization process. Maute and Ramm [27] proposed an adaptive scheme to separate the design optimization and analysis models. They performed shape and topology optimization separately and mapped the results to each other. They employed the adaptive mesh refinement strategy on the finite element mesh to change the design patch of the topology optimization. Kim and Yoon [28] utilized wavelet space to perform the design optimization progressively from low to high resolution while using the same finite element mesh. Moreover, Kim *et al*. [29] developed a multiscale wavelet-Galerkin method and used it as an adaptive solver. The analysis and the design optimization are integrated in a multiresolution framework so that both the analysis resolution and the design resolution can be adaptively adjusted. In their approach, at all levels, the design resolution is similar or coarser than the analysis resolution. Recently, Guest and Genut [30] used a separate design variable mesh and finite element mesh such that the density of the finite element is obtained by projection of the design variables. They utilized the finite element mesh and an adaptive design variable field where the design variables can be activated and deactivated during the optimization process depending on the structural regions. This approach provides the optimal design that has the same resolution with the finite element mesh [30]. The proposed adaptive multiresolution topology optimization (AMTOP) approach in this paper is based on the iMTOP scheme described in the first part. The motivation for the adaptive approach is to use iMTOP elements only where and when needed; otherwise, the conventional elements are used — the finite element mesh stays the same during the optimization process.

The remainder of this paper is structured as follows: Section 2 proposes multiple distinct meshes for improving multiresolution topology optimization; Section 3 describes the formulation for improving multiresolution approach; Section 4 proposes the adaptive multiresolution topology optimization procedure; Section 5 provides two-dimensional (2D) examples; Section 6 provides three-dimensional (3D) examples; and finally Section 7 concludes the paper.

2. MULTIPLE DISCRETIZATIONS FOR TOPOLOGY OPTIMIZATION

Existing topology optimization approaches such as the element-based and nodal-based approaches can be interpreted with a design variable mesh and a finite element (displacement) mesh. For example, the element-based approach considers a uniform density of each finite element as a design variable for optimization as shown in Figure 2(a). By contrast, the nodal-based approaches [14–16] consider the densities at the finite element nodes as the design variables. Another option is to locate the nodal design variables at the midpoints of the four edges of the quadrilateral elements [17]. The design variables can be independent of the finite element mesh and can be adaptively reduced during the topology optimization process [30]. In the above-mentioned approaches, the topology design is defined via the density of the finite element mesh. Therefore, the highest achievable resolution is that of the finite element mesh.

Recently, Nguyen *et al*. [20] proposed the use of three meshes: finite element mesh, design variable mesh, and density element mesh for multiresolution topology optimization. For example, each Q4 element is divided into a number of density elements (e.g., $n = 25$). Design variable is defined as the density at the center of the density element. The number of design variables, therefore, equals the number of density elements as shown in Figure 2(b). The uniform density of a density element is computed from the values of the design variables via a projection function.

DOI: 10.1002/nme

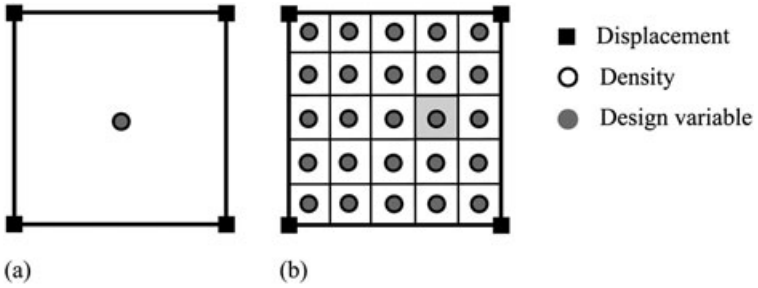

Figure 2. Topology optimization elements: (a) Element-based approach (Q4/U); and (b) MTOP approach (Q4/n25).

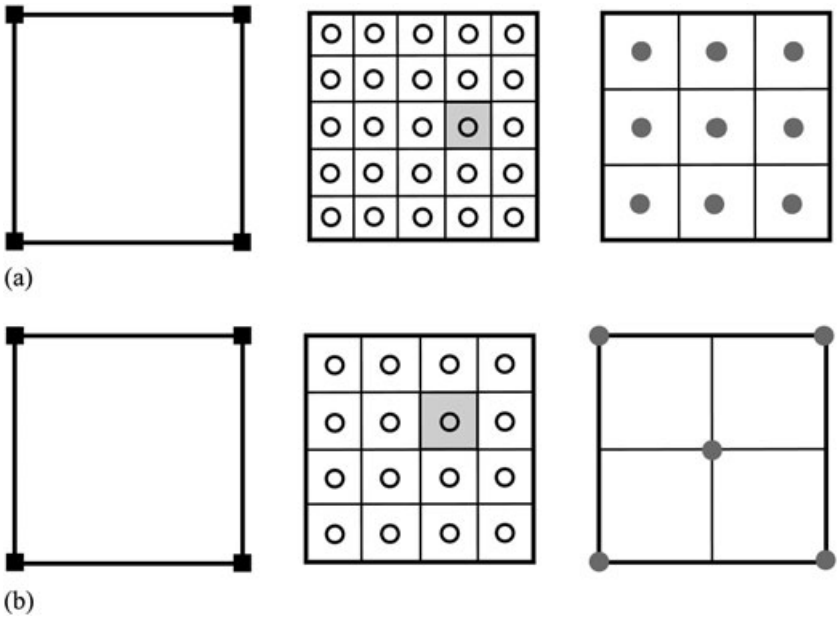

Figure 3. iMTOP elements: (a) Q4/n25/d9 element; and (b) Q4/n16/d5 element.

2.1. Finite element, density and design variable meshes

Here, we present an efficient procedure for improving multiresolution topology optimization (denoted as iMTOP). A relatively coarse mesh is employed for finite elements, a moderately fine mesh for design variables, and a relatively fine mesh for density elements. In comparison to our previous study (MTOP; [20]), we use fewer design variables, therefore, the computational cost can be further reduced in the optimization, sensitivity analysis and projection. For example, Figure 2(a) shows the element-based approach with Q4/U element while Figure 2(b) shows Q4/n25 element where $n = 25$ is the number of density elements/design variables per Q4 finite element. With the proposed improvement, we use fewer design variables per Q4 element than in Figure 2(b). For instance, Figure 3(a) shows the proposed iMTOP element: Q4/n25/d9 where $n = 25$ and $d = 9$ are the number of density elements and design variables, respectively. The number of design variables in Q4/n25/d9 element (Figure 3(a)) is relatively smaller than that in the original Q4/n25 element (Figure 2(b)). Figure 3(b) shows another choice of density elements and design variables (Q4/n16/d5).

2.2. iMTOP elements for two-dimensional and three-dimensional topology optimization

The concept of three distinct meshes can be applied to other two-dimensional and three-dimensional element types in which the number of design variables is less than the number of density elements. For two-dimensional problems, Figure 4(a) shows triangular element with 16 density elements per

DOI: 10.1002/nme

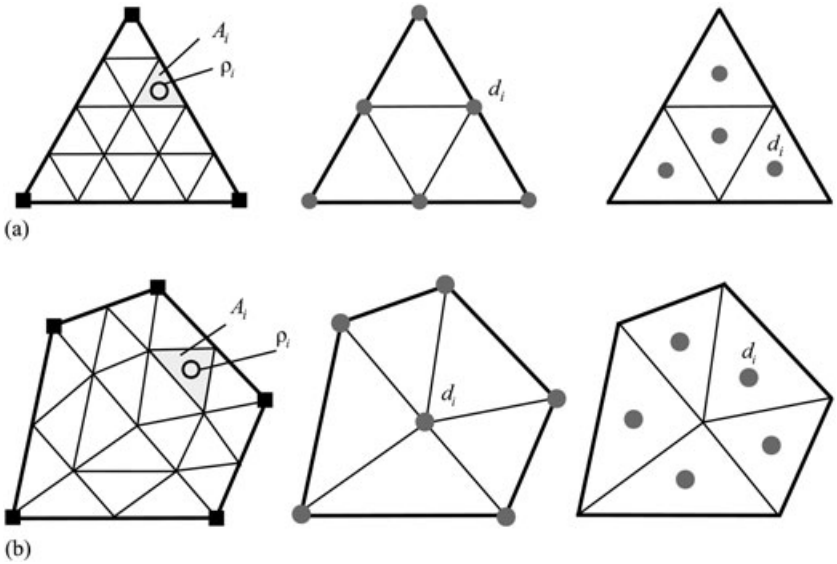

Figure 4. Two-dimensional iMTOP elements: (a) triangular T3/n16/d6 and T3/n16/d4 elements; and (b) polygonal P5/n20/d6 and P5/n20/d5 elements.

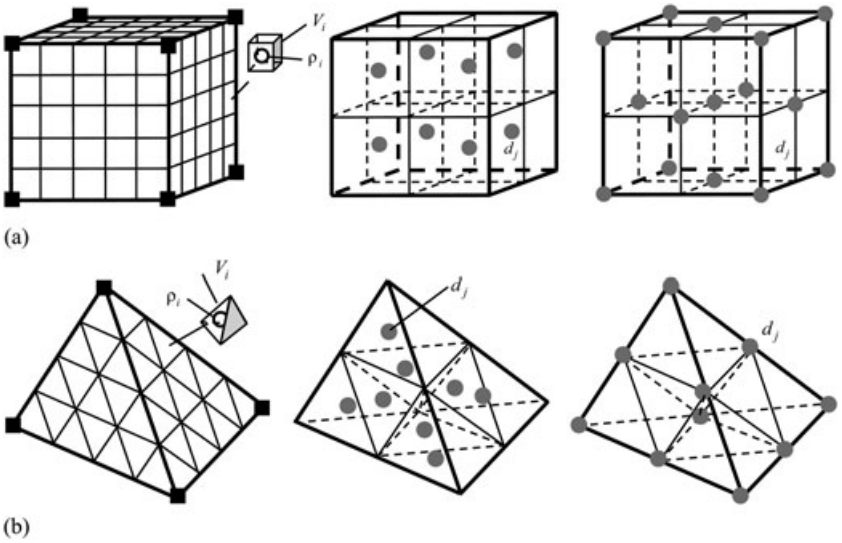

Figure 5. Three-dimensional iMTOP elements: (a) brick B8/n125/d8 and B8/n125/d15 elements; and (b) tetrahedral TET4/n64/d8 and TET4/n64/d10 elements.

finite element and 6 or 4 design variables to create T3/n16/d6 or T3/n16/d4 elements, respectively. We can also apply the iMTOP approach to polygonal finite elements [31] to improve the resolution design. For example, Figure 4(b) shows a polygonal element with five edges (P5) using $n = 20$ density elements. We introduce here P5/n20/d6 and P5/n20/d5 elements where 6 and 5 are the number of design variables per polygonal element, respectively. For three-dimensional problems, Figure 5(a) shows 125 density elements per B8 element with 8 and 15 design variables, denoted by B8/n125/d8 and B8/n125/d15; and Figure 5(b) shows 64 density elements of a tetrahedral element with 8 and 10 design variables, denoted as TET4/n64/d8 and TET4/n64/d10, respectively. It is noteworthy that the iMTOP elements in this paper utilize the locations of design variables associated with the finite elements to develop systematic element types. We actually can use the design

DOI: 10.1002/nme

variables located at any points in the design space [32]. Thus, future work may seek the optimal number and locations of the design variables.

2.3. Projection of design variables to density elements: a minimum length scale approach

Studies have been conducted to improve the manufacturability of the topology design and alleviate the numerical instability [33–36]. Imposing a prescribed length scale feature might also alleviate numerical instability and checkerboard effect. Mesh independent filtering techniques have been developed as restriction methods for the density-based topology optimization such as the sensitivity filter [37], density filter [38, 39], and projection function [14]. For comparison of the filtering techniques, readers are referred to the Reference [40]. The latter two approaches have some similarity; the density filter method in [38] uses the finite element density design variables, while the projection method in [14] uses the finite element nodal design variables. In our study, we refer to the approach as the projection method [14, 41] to compute the element density from the design variables. The projection method uses the design variables associated with the design variable mesh to compute the element densities that belong to the density element mesh.

Here, d_n denotes the design variable associated with the design variable mesh, and ρ_i represents the density of element i associated with the density element mesh. If the change of material density occurs over a minimum length $r_{\min}$, as shown in Figure 6, then the element density ρ_i is obtained from the design variable d_n as

$$\rho_i = f(d_n), \tag{1}$$

where $f(.)$ denotes the projection function. For example, if a linear projection is employed, the uniform density of a density element is computed as the weighted average of the design variables in the neighborhood as follows:

$$\rho_i = \frac{\sum_{n \in S_i} d_n w(r_{ni})}{\sum_{n \in S_i} w(r_{ni})}, \tag{2}$$

where S_i is the subdomain associated with density element i, as shown in Figure 6, and r_{ni} is the distance from the point associated with design variable d_n to the centroid of density element i. The corresponding weight function is defined as

$$w(r_{ni}) = \begin{cases} \frac{r_{\min} - r_{ni}}{r_{\min}} & \text{if } r_{ni} \leqslant r_{\min} \\ 0 & \text{otherwise} \end{cases}. \tag{3}$$

Note that the physical radius $r_{\min}$ (see Figure 6) is independent of the mesh. Using the projection function with a minimum length scale, one thus obtains a mesh independent solution.

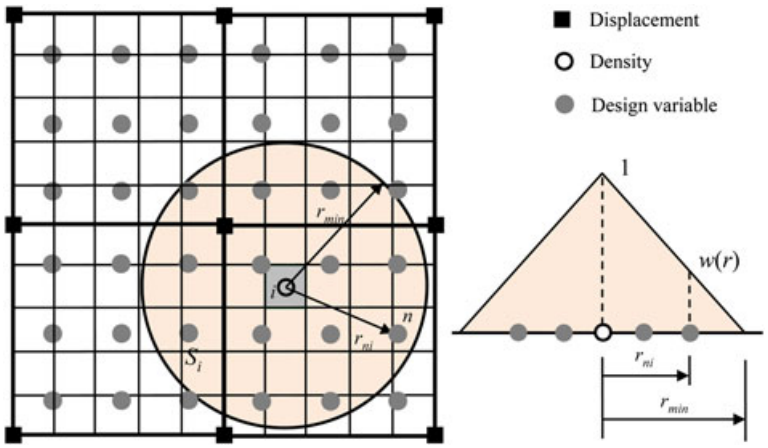

Figure 6. Projection function from the design variables to the density element (Q4/n25/d9).

DOI: 10.1002/nme

3. IMPROVING MULTIRESOLUTION TOPOLOGY OPTIMIZATION FORMULATION

In this section, the problem formulation for iMTOP is presented. For illustration purposes, a compliance optimization problem is considered in which the compliance is minimized under a volume constraint.

3.1. Problem statement and formulation

The basic problem statement is expressed in the discrete form using finite element method as follows:

$$\begin{aligned} \min_{\mathbf{d}} \quad & C(\rho, \mathbf{u}) = \mathbf{f}^{\mathrm{T}}\mathbf{u} \\ \text{s.t.}: \quad & \rho = f(\mathbf{d}) \\ & \mathbf{K}(\rho)\mathbf{u} = \mathbf{f} \\ & V(\rho) = \int_{\Omega} \rho \mathrm{d}V \leqslant V_s \\ & 0 < \rho_{\min} \leqslant \mathbf{d} \leqslant 1 \end{aligned}, \tag{4}$$

where C is the compliance, $\mathbf{d}$ is the vector of design variables, $f(.)$ is the projection function, $\rho = \rho(\mathbf{x})$ is the density at position $\mathbf{x}$, respectively, $\mathbf{K}$ is the global stiffness matrix, V_s is the prescribed volume, and $\mathbf{f}$ and $\mathbf{u}$ are the global load and displacement vectors. The desirable solution indicates whether the density at any point in the domain is either 0 (void) or 1 (solid). However, it is impractical or computationally intractable to solve the integer optimization problem [42]. In a relaxed problem, the density can have an intermediate value between 0 and 1. For example, in the popular solid isotropic material with penalization (SIMP) [3, 43, 44] model, Young's modulus is parameterized using solid material density as follows:

$$E(\mathbf{x}) = \rho(\mathbf{x})^p E^0, \tag{5}$$

where E^0 is the original Young's modulus of the material in the solid phase, corresponding to the density $\rho = 1$, and the exponent p is the penalization parameter. To prevent singularity of the stiffness matrix, a small positive lower bound, for example, $\rho_{\min} = 10^{-3}$, is placed on the density. When the penalization parameter p is greater than 1, the intermediate density approaches either 0 (void) or 1 (solid). We also impose the same density bounds on the design variables $\mathbf{d}$ in Equation (4).

3.2. Integration of stiffness matrix

In the traditional element-based approach, the density of each finite element is represented by one value ρ_e and the global stiffness matrix $\mathbf{K}$ is expressed as

$$\mathbf{K} = \sum_{e=1}^{N_{el}} \mathbf{K}_e(\rho) = \sum_{e=1}^{N_{el}} \int_{\Omega_e} \mathbf{B}^{\mathrm{T}}\mathbf{D}(\rho)\mathbf{B}\mathrm{d}\Omega, \tag{6}$$

where $\mathbf{K}_e(\rho)$ is the stiffness matrix of the element e, $\mathbf{B}$ is the strain–displacement matrix (shape function derivatives), and $\mathbf{D}(\rho)$ is the constitutive matrix, which depends on the material density ($\mathbf{D}(\rho) = \rho^p\mathbf{D}^0$ where $\mathbf{D}^0$ is the constitutive matrix of the solid material).

By contrast, in the iMTOP approach, each finite element consists of a number of density elements, and the density is assumed to be uniform inside each density element. The stiffness matrix of the finite element is computed as the summation of the integration of the stiffness integrand over each density element. For example, for a Q4 element with unit thickness, the formulation to compute the stiffness matrix in the reference domain is as follows [45]:

$$\mathbf{K}_e = \int_{\Omega_e} \mathbf{B}^{\mathrm{T}}\mathbf{D}\mathbf{B}\mathrm{d}\Omega = \int_{-1}^{1}\int_{-1}^{1} \mathbf{B}^{\mathrm{T}}\mathbf{D}\mathbf{B}J\,\mathrm{d}\xi\mathrm{d}\eta, \tag{7}$$

DOI: 10.1002/nme

where (ξ, η) denote the intrinsic coordinates in the interval [–1,1], J is the Jacobian, and $\mathbf{B}$ is the strain–displacement matrix in the reference (parent) domain. The standard formulation of matrix $\mathbf{B}$ in the reference domain can be found in the literature [45]. The integration of the stiffness matrix integrand over the reference domain Ω_0 (Figure 7) can be computed as follows:

$$\mathbf{K}_e = \sum_{i=1}^{N_n} \left(\int_{\Omega_i^0} \mathbf{B}^{\mathrm{T}} \mathbf{D} \mathbf{B} J \, \mathrm{d}\xi \mathrm{d}\eta \right) = \sum_{i=1}^{N_n} \left(\int_{\Omega_i^0} \mathbf{B}^{\mathrm{T}} \mathbf{D} \mathbf{B} J \, \mathrm{d}\Omega_i^0 \right), \tag{8}$$

where Ω_i^0 is the domain of the density element i (area A_i^0 for 2D, and volume V_i^0 for 3D) in the reference domain Ω_0 and N_n is the number of the integration elements in the displacement element domain. Note N_n is also equal to the number of density elements per displacement element, $N_n = n$.

The SIMP interpolation model is employed to evaluate the stiffness matrix in (8) as follows:

$$\mathbf{K}_e = \sum_{i=1}^{N_n} \left((\rho_i)^p \int_{\Omega_i^0} \mathbf{B}^{\mathrm{T}} \mathbf{D}^0 \mathbf{B} J \, \mathrm{d}\Omega_i^0 \right) = \sum_{i=1}^{N_n} (\rho_i)^p \mathbf{I}_i, \tag{9}$$

where $\mathbf{D}^0$ is the constitutive matrix corresponding to the solid phase and $\mathbf{I}_i$ is

$$\mathbf{I}_i = \int_{\Omega_i^0} \mathbf{B}^{\mathrm{T}} \mathbf{D}^0 \mathbf{B} J \, \mathrm{d}\Omega_i^0. \tag{10}$$

When a large number of density elements are employed in a displacement element (e.g. $n = 25$ for Q4 element, $n = 125$ for B8 element), the integration of the stiffness matrix in (9) can be approximated by the summation of the integrand evaluated at the center of each density element [20, 32]. Thus, the integral (10) can be simplified as

$$\mathbf{I}_i = \left(\mathbf{B}^{\mathrm{T}} \mathbf{D}^0 \mathbf{B} J \right) \big|_i \, A_i^0 \, . \tag{11}$$

Figure 8(a) shows a Q4 with 25 density elements, Figure 8(b) shows the exact integration scheme in (10), and Figure 8(c) shows the approximated integration scheme in (11).

3.3. Sensitivity

The solution of the gradient-based optimization problem (4) requires the computation of sensitivities of objective function and constraint. The sensitivity of the compliance requires the computation of the sensitivity of the stiffness matrix with respect to the design variable, which can be

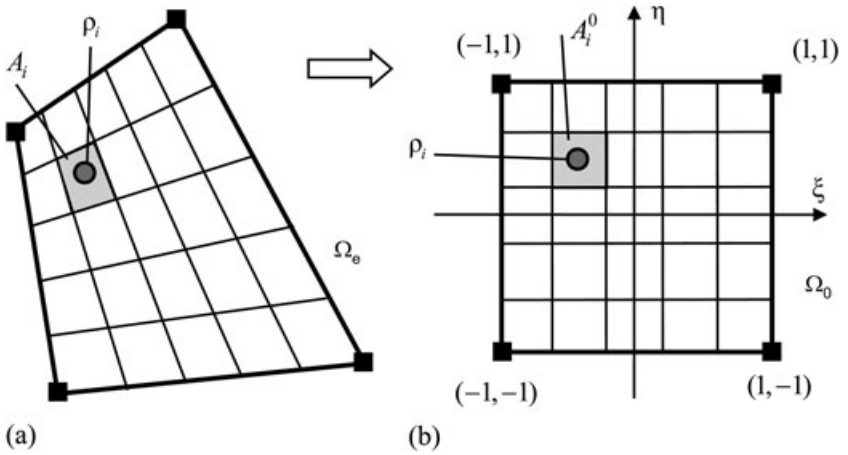

Figure 7. Isoparametric element: (a) initial domain; and (b) reference domain.

DOI: 10.1002/nme

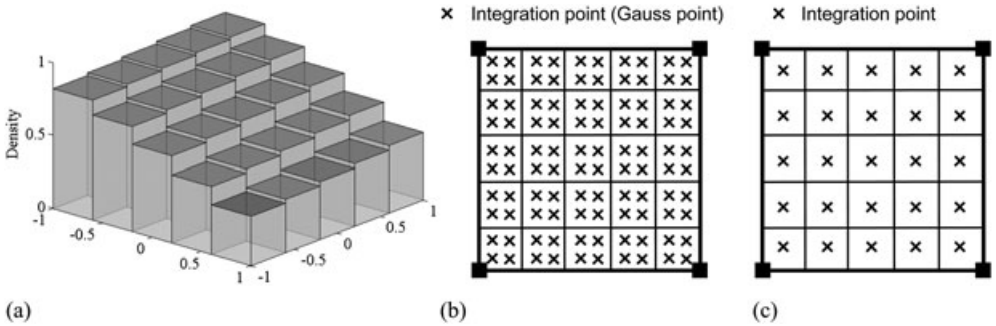

Figure 8. Integration points for Q4/n25 element: (a) spatial distribution of the density; (b) Gauss quadrature; and (c) approximation.

calculated as

$$\frac{\partial \mathbf{K}_e}{\partial d_n} = \sum \frac{\partial \mathbf{K}_e}{\partial \rho_i}\frac{\partial \rho_i}{\partial d_n} = \sum \frac{\partial \left(\sum_{j=1}^{N_n} (\rho_j)^p \mathbf{I}_j \right)}{\partial \rho_i}\frac{\partial \rho_i}{\partial d_n} = \sum (\rho_i)^{p-1}\mathbf{I}_i \frac{\partial \rho_i}{\partial d_n}, \tag{12}$$

where d_n and ρ_i are the design variable and element density, respectively. The sensitivities of the compliance and the volume are computed as follows:

$$\begin{aligned} \frac{\partial C}{\partial d_n} &= \sum \frac{\partial C}{\partial \rho_i}\frac{\partial \rho_i}{\partial d_n} = \sum -\mathbf{u}^{\mathrm{T}}\frac{\partial \mathbf{K}}{\partial \rho_i}\mathbf{u}\frac{\partial \rho_i}{\partial d_n} \\ \frac{\partial V}{\partial d_n} &= \sum \frac{\partial V}{\partial \rho_i}\frac{\partial \rho_i}{\partial d_n} = \int_{\Omega_i} \mathrm{d}V \frac{\partial \rho_i}{\partial d_n} \end{aligned}. \tag{13}$$

The sensitivities of the element density with respect to design variables are derived as

$$\frac{\partial \rho_i}{\partial d_n} = \frac{w(r_{ni})}{\sum_{m\in S_i} w(r_{mi})}. \tag{14}$$

The above derivation of sensitivity analyses of the compliance and volume constraint are for the minimum compliance problem. When other topology optimization problems such as 'compliant mechanism' [42, 46] are considered, the objective function and constraints are derived from the chain rule. For example, if an objective function or constraint is described as a function of the density such as displacement, that is, $g(\rho)$, then the sensitivity of this function with respect to the design variable is computed as follows:

$$\frac{\partial g(.)}{\partial d_n} = \sum \frac{\partial g(.)}{\partial \rho_i}\frac{\partial \rho_i}{\partial d_n}. \tag{15}$$

3.4. iMTOP ratio — measuring efficiency and resolution

The efficiency of a topology optimization model can be measured directly using the normalized computer run time. However, this comparison may not be always appropriate. For example, one may employ a very fast solver, and then the computational cost of the element-based approach on fine mesh will get closer to that of the MTOP approach. Also, implementation of the code in different programming languages may also lead to different efficiency levels. The efficiency depends on code structures as well. Thus, we need a measure to describe and compare the efficiency and resolution in terms of the number of finite elements, density elements and design variables. Table I compares the iMTOP elements with the conventional element-based approach. First, the total number of finite elements is related to the total degrees of freedom in the linear equations of equilibrium. Second, the number of density elements determines the resolution of the design. In the element-based

DOI: 10.1002/nme

Table I. Summary iMTOP ratio of elements.

			Number of			
	Approaches	Element types	Finite elements	Density elements	Design variables	iMTOP ratio k: n: d
2D: Q4	Element-based	Q4/U	1	1	1	1 : 1 : 1
	MTOP	Q4/n25	1	25	25	1 : 25 : 25
	iMTOP	Q4/n25/d9	1	25	9	1 : 25 : 9
		Q4/n25/d4	1	25	4	1 : 25 : 4
3D: B8	Element-based	B8/U	1	1	1	1 : 1 : 1
	MTOP	B8/n125	1	125	125	1 : 125 : 125
	iMTOP	B8/n125/d15	1	125	15	1 : 125 : 15
		B8/n125/d8	1	125	8	1 : 125 : 8

approach, each finite element contains one density element whereas in the super-element approach, each density element represents the densities of several neighboring finite elements. By contrast, in the iMTOP approach, each finite element consists of a number of density elements. When the number of density elements increases, the resolution of the design increases. However, the computational cost related to stiffness matrix calculation, sensitivity analysis, and projection increases as well. Finally, the number of design variables determines the computational cost in optimization, sensitivity analysis, and projection. A ratio is introduced to measure the efficiency and resolution of an iMTOP element type, termed as the 'iMTOP ratio', which is defined as follows:

$$\text{iMTOP ratio} = k\ :\ n:\ d = \begin{array}{l}\text{(the number of finite elements) : (the number of density}\\ \text{elements) : (the number of design variables)}\end{array}. \tag{16}$$

For models with the same number of finite elements (k), the larger the number of density elements (n) is, the higher resolution is obtained. On the other hand, a smaller number of density elements and design variables indicate higher efficiency. Therefore, when models are considered with the same number of finite elements (k), it is desirable to have a larger number of density elements (n) and a smaller number of design variables (d). Table I shows the iMTOP ratio for element-based, MTOP, and iMTOP approaches.

4. ON ADAPTIVE MULTIRESOLUTION TOPOLOGY OPTIMIZATION

We hereby present a heuristic adaptive scheme that can be used in conjunction with multiresolution topology optimization. The motivation is to further reduce the design space by reducing the number of design variables and/or density elements in the multiresolution framework. For more detailed accounts on adaptivity theory and approaches, the readers are referred to the literature [24–26, 47]. Here our approach focuses on selective adjustment of the design space for topology optimization.

4.1. Reducing design variable and density fields

We propose here a simple and heuristic adaptive multiresolution topology optimization (AMTOP) procedure, which is based on the scheme described in Section 2. As demonstrated by means of numerical examples, the approach leads to high resolution design with relatively low computational cost by using iMTOP elements (e.g., Q4/n25/d4) rather than conventional elements (e.g., Q4/U). However, we only use iMTOP elements where and when needed; otherwise, we use conventional elements (e.g., Q4/U). During the optimization process, some regions may have uniform material distribution such as void regions or solid regions. In the regions where material distribution is uniform, the iMTOP elements (e.g., Q4/n25/d4) are replaced by the conventional elements (e.g., Q4/U). On the other hand, the iMTOP elements are used in regions where the material density gradient is high. In these regions, structural boundaries are forming, and therefore we need a higher resolution to represent the material distribution.

DOI: 10.1002/nme

4.2. Adaptive multiresolution design space

The adaptive scheme consists of using iMTOP elements only in the regions where they are needed; otherwise, conventional elements are used via a criterion based either on design variables or on density elements. The procedure is shown here in terms of density elements. For illustrative purpose, Q4/U and Q4/$n25/d4$ elements are used in the explanation; however, more than one type of iMTOP elements can be used in a particular optimization problem. During the optimization process, element types are tracked using an 'element index array.' Each finite element e is assigned an 'element index' ei, where $ei = 1$ indicates a conventional element (e.g., Q4/U), and $ei = n$ (e.g., $n = 25$) indicates an iMTOP element (e.g., Q4/$n25/d4$).

Initially, when the material distribution is uniform, all elements are assigned as conventional ones (e.g., Q4/U). The optimization is performed until the objective function is converged. The iMTOP element type is determined for each finite element based on element densities. We propose an alternative approach that determines the element type based on the gradient of the material density. For example, iMTOP elements are used where the material density gradient is relatively high and conventional elements are used where the material is relatively more uniform. However, in the current implementation, an element e is changed from conventional to iMTOP when it is sufficiently 'gray', that is, $\rho_L < \rho_e < \rho_U$, where ρ_L and ρ_U are predefined thresholds, for example, $\rho_L = 0.015$ and $\rho_U = 0.99$. On the other hand, an iMTOP element is changed to conventional when all of their densities are sufficiently 'black' or 'white', that is, $\rho_i > \rho_U$ or $\rho_i < \rho_L$. The 'element index' ei is then updated whenever the element is changed either from iMTOP to conventional or from conventional to iMTOP. The criteria for the above element type updating scheme is based on the convergence of the objective function. For example, the element type is updated if the relative change of the objective function is less than a threshold (e.g., 1%) after a certain number of optimization iterations (e.g., 20). The process of element type updating and optimization iterations are repeated until the convergence criteria on maximum number of iterations (e.g., 100 iterations) or the relative change in the objective function (e.g., 0.1%) is satisfied. The flow chart of the adaptive procedure is explained in Figure 9.

In summary, an adaptive procedure is proposed to utilize the iMTOP elements only in the selected regions in the domain during the optimization process using a simple algorithm. The procedure is demonstrated via numerical examples in the subsequent sections. Our proposed adaptive approach has some similarity with the adaptive approach of Reference [30] in that both approaches keep the same finite element mesh during the optimization process. However, while the approach of Reference [30] utilizes a coarser design variable mesh than the finite element mesh, our approach consists of the opposite in the sense that we use a finer design variable mesh. In addition, the resolution of the design (density element mesh) in our approach is adaptively changed and finer than the finite element mesh during optimization process while the approach of Reference [30] maintains the design resolution always the same as the finite element mesh (one density element per finite element). As indicated, our proposed adaptive approach is the opposite of the one of Reference [30].

5. TWO-DIMENSIONAL NUMERICAL EXAMPLES

In this section, the proposed approaches are demonstrated with various two-dimensional applications. First, the minimum compliance problem of a beam under a concentrated load is considered (Figure 10(a)). Second, the compliant mechanism design of a displacement inverter is investigated (Figure 10(b)). Third, a cantilever beam is investigated to demonstrate the adaptive procedure. In these examples, the SIMP model is employed to interpolate the stiffness tensor of the intermediate material density. The method of moving asymptotes (MMA) [48] is used as the optimizer. For simplicity, all the quantities are given dimensionless. Thus, Young's modulus is chosen as 1 and Poisson's ratio as 0.3 for all examples. Instead of using prescribed volume constraint V_s, we use volume fraction *volfrac*, which is defined as the ratio of the prescribed volume V_s to the total volume of the domain. All the computations are performed on a single PC with an Intel Core(TM)2 Duo 2.00 GHz 32-bit processor, 3 GB RAM of memory, Windows OS, and the code is implemented in MATLAB.

DOI: 10.1002/nme

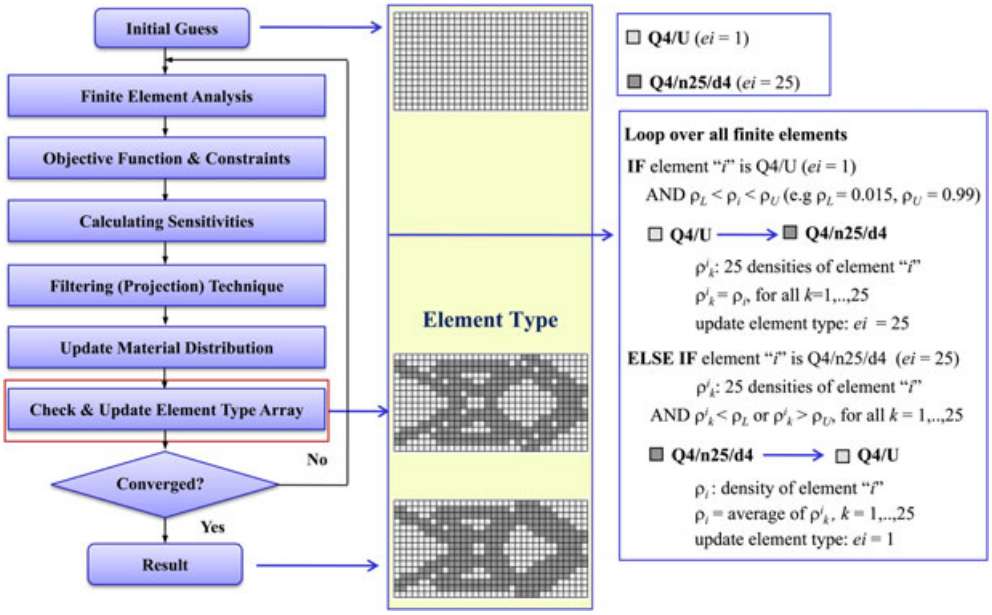

Figure 9. Flow chart of the adaptive MTOP scheme (Q4/n25/d4 and Q4/U).

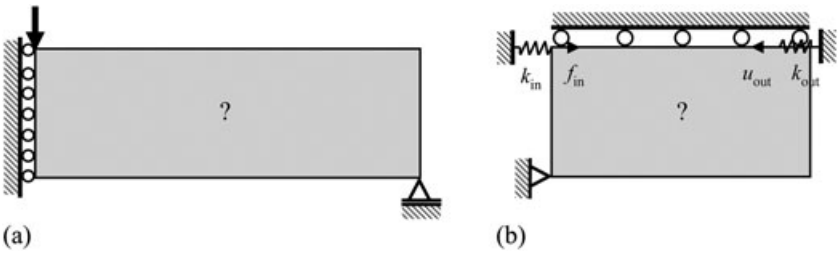

Figure 10. Configurations: (a) MBB beam; and (b) displacement inverter.

5.1. Minimum compliance of a Messerschmitt–Bolkow–Blohm beam

This example presents the solution for minimum compliance of a beam subjected to a concentrated vertical load, the so-called Messerschmitt–Bolkow–Blohm (MBB) beam. Because of the symmetry, only half of the beam is taken into consideration with the length of 60, height of 20, and unit width as shown in Figure 10(a). The volume fraction constraint *volfrac* is taken as 60%, the penalization parameter p is set equal to 3, and the projection radius $r_{\min}$ is set equal to 1/10 of the height of the beam.

First, the element-based topology optimization is performed on a fine FE mesh of 300×100 and a coarse FE mesh of 60×20 Q4/U elements — the optimal topologies are shown in Figures 11(a) and (b), respectively. The topology obtained from the fine FE mesh has higher resolution than that from the coarse mesh. Next, we utilize the previous MTOP approach [20] using 60×20 Q4/n25 elements and obtain the topology shown in Figure 11(c). The topologies in Figures 11(a) and (c) have higher resolution than the topology in Figure 11(b) obtained from a coarse FE mesh.

Second, using the iMTOP approach, we vary the number of design variables for the same resolution (or the same number of density elements). Instead of using MTOP Q4/n25 elements where the number of design variables equals to the number of density elements, we reduce the number of design variables per Q4 finite element to 16, 9, and 4. As a result, we have a coarse FE mesh of 60×20, a fine density element mesh of 300×100, and the design variable meshes of 240×80, 180×60, and 120×40, respectively. The optimal topologies shown in Figures 11(d), (e) and (f) correspond to iMTOP Q4/n25/d16, Q4/n25/d9, and Q4/n25/d4 elements, respectively. These topologies

DOI: 10.1002/nme

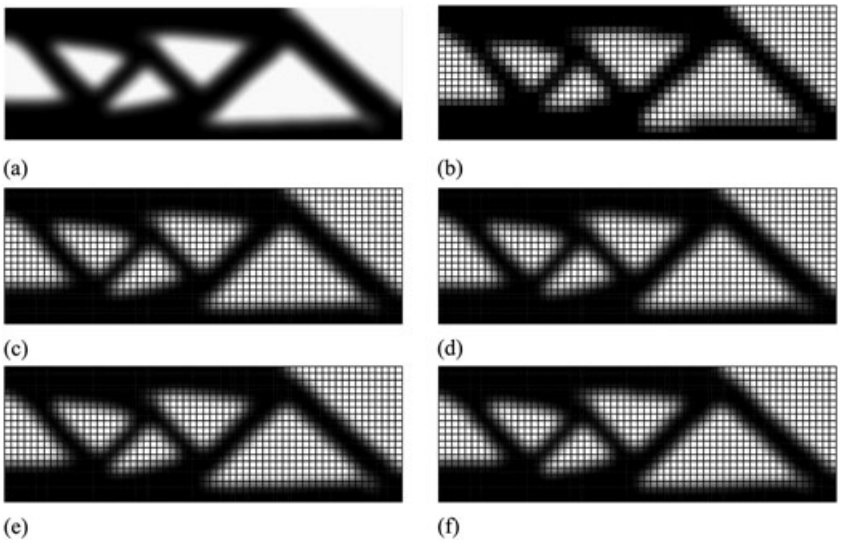

Figure 11. Optimal topologies of MBB beam: (a) element-based Q4/U FE mesh 300×100 (C=187.71); (b) element-based Q4/U FE mesh 60×20 (C = 181.04); (c) MTOP Q4/n25 (C = 181.90); (d) iMTOP Q4/n25/d16 (C = 181.95); (e) iMTOP Q4/n25/d9 (C = 181.99); and (f) iMTOP Q4/n25/d4 (C = 181.96)

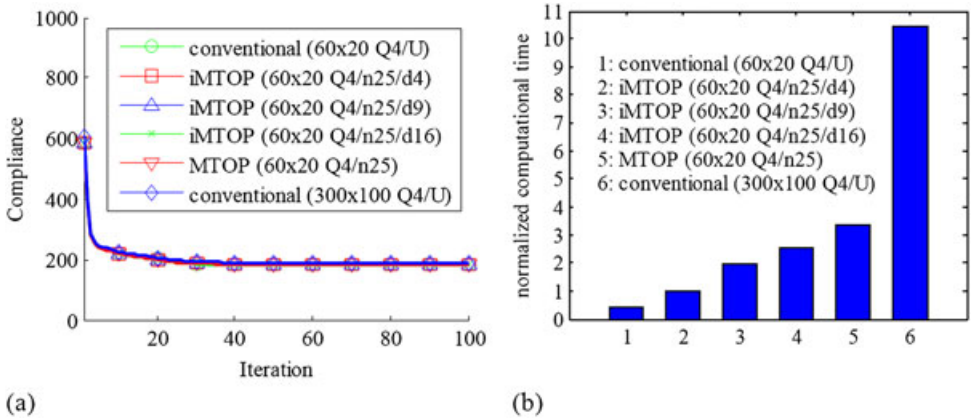

Figure 12. Results of MBB beam optimization after 100 iterations: (a) convergence history; and (b) computational times.

are similar to the optimal topology obtained with MTOP Q4/n25 elements in Figure 11(c). Moreover, we can observe close values of compliances of the optimal topologies that are obtained by the same number of density elements and different number of design variables.

In this example, the approximate integration of the stiffness matrix in Equation (11) is used for the multiresolution approach. The optimal topology in Figure 11(c) is obtained using MTOP Q4/n25 with 25 integration points and the corresponding optimal compliance is $C = 181.90$. Finite element analysis using MTOP elements is performed on the topology in Figure 11(c) using the exact integration in (10), 4 Gauss points for each density element, so that each MTOP Q4/n25 element employs 100 Gauss points. The resulting compliance of 181.52 is obtained, which is only 0.21% different from the approximation scheme in Equation (11). Although more tests are needed, these results indicate that the approximation scheme in Equation (11) may be useful in practice because of its simplicity and uniform applicability.

The convergence history of the iMTOP and the element-based approaches are compared in Figure 12(a). During the optimization process, the compliance convergence history from the iMTOP and element-based approaches are very similar. The computational costs are compared in

DOI: 10.1002/nme

Figure 12(b). As expected, the element-based approach on a fine mesh has the largest computational cost. The lower computational cost for iMTOP approach is attributed to a lower number of finite elements, in comparison to element-based approach on a fine FE mesh, and a lower number of design variables, in comparison to MTOP approach on the same FE mesh. Figure 12(b) shows that MTOP Q4/$n25$ is about three times less expensive than the element-based approach on a fine mesh. Moreover, the computational cost is further reduced for iMTOP Q4/$n25$/$d16$, Q4/$n25$/$d9$, and Q4/$n25$/$d4$. In this example, the computational cost of iMTOP Q4/$n25$/$d4$ is about 3.5 times less than that of MTOP Q4/$n25$ and about 10 times less than that of the element-based approach on a fine mesh. The computational cost saving in iMTOP Q4/$n25$/$d4$ is attributed to a much less number of design variables in comparison to that of MTOP Q4/$n25$. Therefore, the cost in the MMA optimization, the sensitivity analysis, and the projection is also reduced.

The MBB example is further investigated using a minimum length scale equal to 5% of the height of the beam. First, for the same coarse FE mesh, the element-based approach results in undesirable checker board effects (Figure 13(b)); while the MTOP and iMTOP approaches (Figures 13(c) and (d)) provide results comparable to the element-based approach on a fine mesh (Figure 13(a)). This is because the element-based approach cannot utilize a length scale smaller than or equal to the element size while both MTOP and iMTOP approaches can. Second, the optimal topology by iMTOP Q4/$n25$/$d4$ in Figure 13(d) is slightly different from that by MTOP Q4/$n25$. However, these two designs have close optimal objective function values. The difference of these two optimal objective functions is only 0.3%. Thus, these results demonstrate the advantages of the iMTOP and MTOP approaches over the element-based approach when the same coarse FE mesh is employed.

One may refine the finite element mesh to obtain the topology with smooth material boundaries. The MBB example shows that we achieve this desirable effect (smooth boundaries) with our algorithm without having to refine the finite element mesh as shown in Figure 11. Additionally, Figure 13 shows that our algorithm can generate a fine structural resolution when the traditional element based algorithm results in checkerboard. Specifically, by using iMTOP elements, for example, Q4/$n25$/$d4$, we can obtain high resolution topology comparable to MTOP Q4/$n25$ and the element-based approach on a fine mesh with lower computational cost.

5.2. Compliant mechanism of a displacement inverter

The second example presents a 2D compliant mechanism problem, a displacement inverter as shown in Figure 10(b). The goal is to design a structure to convert the input displacement on the left edge to a displacement on the right. The topology optimization seeks for the solution of maximum output displacement with a certain volume fraction of the domain. In this example, we employ a domain of the size 40×20, volume fraction of 0.3 and length scale of 1.2. The input force is $F_{\text{in}} = 1$, the input and output spring stiffnesses are $k_{\text{in}} = k_{\text{out}} = 0.025$.

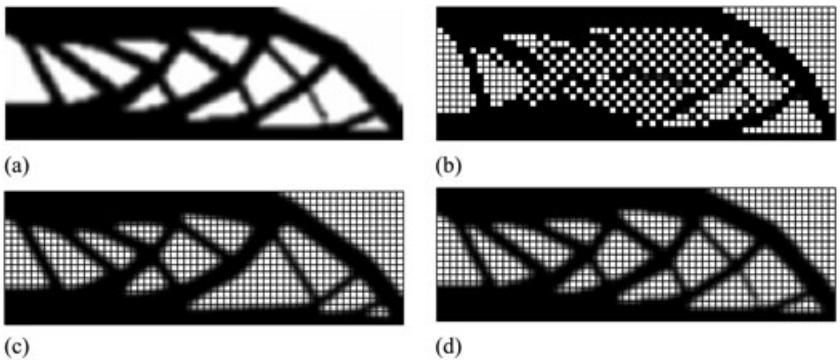

Figure 13. Topologies of MBB beam with rmin = 5% of height of the beam: (a) element-based Q4/U FE mesh 300 × 100 (C = 177.30); (b) element-based Q4/U FE mesh 60 × 20 (C = 163.58); (c) MTOP Q4/n25 (C = 170.48); and (d) iMTOP Q4/n25/d4 (C = 171.07) (b–d: FE mesh 60×20).

DOI: 10.1002/nme

Similarly to the previous example, the element-based approach is performed on a fine mesh of 200×100 Q4 elements and on a coarse mesh of 40×20 Q4 elements. The optimal topologies from a fine mesh and a coarse mesh are shown in Figures 14(a) and (b), respectively. Next, the MTOP approach is performed using Q4/*n*25 elements, and the iMTOP approach is performed using Q4/*n*25/*d*16, Q4/*n*25/*d*9 and Q4/*n*25/*d*4 elements — the optimal topologies are shown in Figures 14(c)–(f), respectively. Similar conclusions in the performance of the proposed approach on the previous MBB example also hold for the displacement converter problem, as shown in Figure 15. It can be seen that the topologies from MTOP and iMTOP approaches using a coarse FE mesh have comparable resolution to the topology from element-based approach using a fine FE mesh, whereas the topology obtained from element-based approach on coarse FE mesh is slightly different. This example illustrates that the proposed iMTOP approach can be applied not only to minimum compliance problems but also to compliant mechanism problems. Note that for the mechanism problem, the numerical results are sensitive to the parameter inputs (e.g., spring stiffnesses, moving limit in the MMA optimizer, etc.); therefore, this problem should be solved with care.

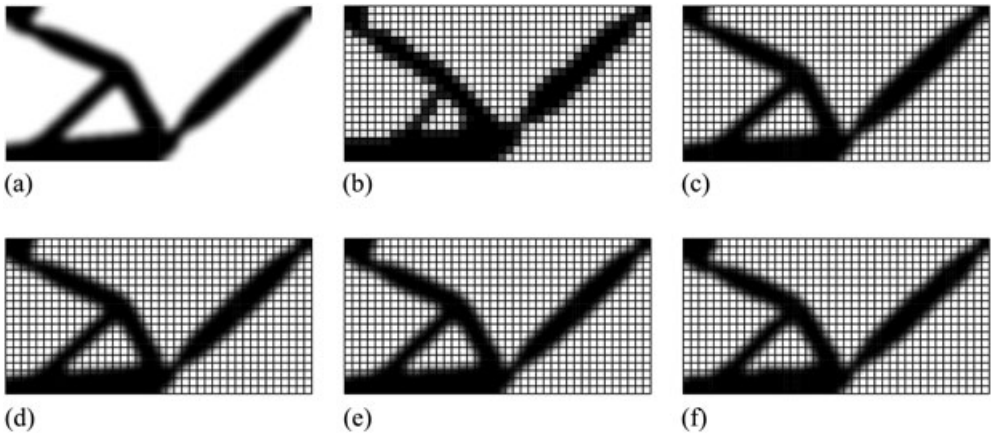

Figure 14. Topologies of the displacement inverter: (a) element-based Q4/U FE mesh 200 × 100 (objective function displacement d = –4.4121); (b) element-based Q4/U FE mesh 40×20 (d = –4.2872); (c) MTOP Q4/n25 (d = –4.2728); (d) iMTOP Q4/n25/d16 (d = –4.2650); (e) iMTOP Q4/n25/d9 (d = –4.2644); and (f) iMTOP Q4/n25/d4 (d = –4.2624) (noted b–f: FE mesh 40×20).

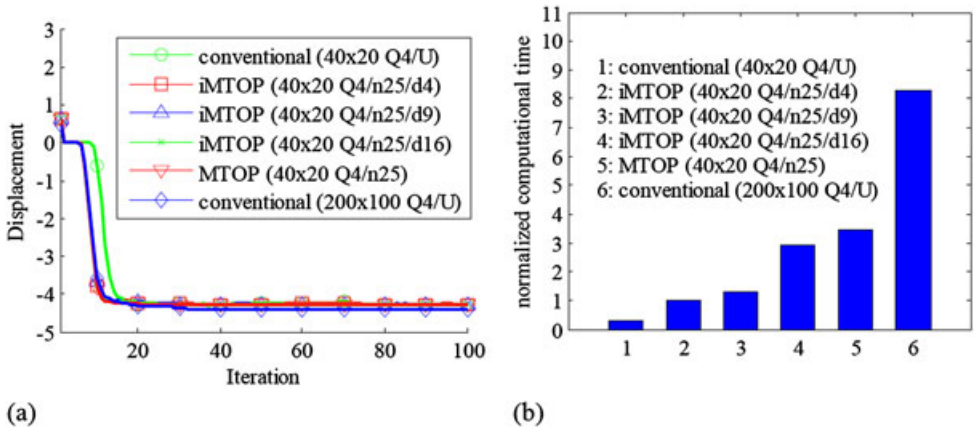

Figure 15. Results of the displacement inverter example after 100 iterations: (a) convergence history; and (b) computational times.

DOI: 10.1002/nme

5.3. Minimum compliance of a cantilever beam

This example demonstrates the adaptive multiresolution topology optimization (AMTOP) procedure proposed in Section 4. A domain with the length of 32, height of 16, and unit width is taken into consideration as shown in Figure 16(a). The beam is fixed at the left edge and a unit point load is applied downward at the midpoint of the right end. A volume fraction constraint *volfrac* is taken as 45%, the penalization parameter p is set equal to 4, and projection radius $r_{\min}$ is set equal to 1.2.

First, the topology optimization of the beam is performed by the element-based approach (Q4/U) on a fine FE mesh and also on a coarse FE mesh with the obtained topologies shown in Figures 16(b) and (c), respectively. The MTOP Q4/n25 and the iMTOP Q4/n25/d4 approaches provide the topologies shown in Figures 16(d) and (e), respectively. Finally, we perform the adaptive procedure using Q4/U and Q4/n25/d4 elements and obtain the results shown in Figure 16(f). Notice that the solution obtained by the adaptive scheme has comparable resolution in comparison to the topologies obtained by MTOP, iMTOP, and element-based approach on a fine mesh.

Figure 17 explains the adaptive optimization process. At the initial stage, we begin the optimization problem with a uniform distribution of the density over the domain. Therefore, only Q4/U elements are employed (a total of 512 elements) as shown in Figure 17(a) with the corresponding topology shown in Figure 17(d) and all the components of the 'element index' array are initialized as 1. As the optimization progresses, for regions with uniform density (void or solid), we use Q4/U elements. At the 'gray' regions, that is, where structural boundaries are forming and thus more information is required, the iMTOP Q4/n25/d4 elements are used to increase the resolution. Figure 17(b) shows the mesh of an intermediate iteration with 244 Q4/U and 268 Q4/n25/d4 elements, and the corresponding topology is shown in Figure 17(e). Figure 17(c) shows the mesh at the final iteration with 222 Q4/U elements and 290 Q4/n25/d4 elements, and the corresponding topology is shown in Figure 17(f). The adaptive procedure to decide where and when to use Q/U or Q4/n25/d4 element is simple because of the 'element index' array described in Section 4.

The iMTOP approach reduces the number of density elements and number of design variables in comparison with the element-based approach on a fine mesh. By employing the adaptive approach, we can further reduce the number of density elements and design variables to achieve higher efficiency. For this specific example, we observe that the computational time for adaptive approach using Q4/U and Q4/n25/d4 elements (Figure 16(f)) is about 70% of that using iMTOP with Q4/n25/d4 elements (Figure 16(e)).

In summary, this example demonstrates that the adaptive procedure can further improve the efficiency of the iMTOP approach while maintaining the design resolution. In this example, Q4/U

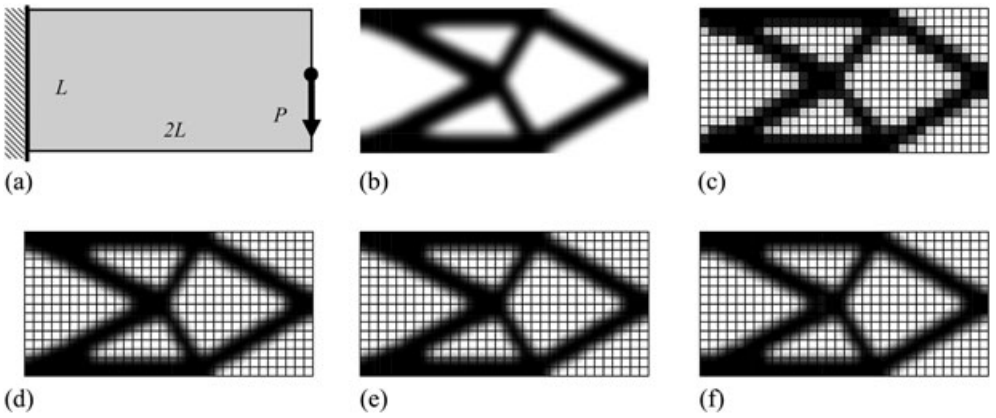

Figure 16. Cantilever example considering adaptive topology optimization: (a) geometry; (b) element-based Q4/U FE mesh 160×80 (C = 90.11); (c) element-based Q4/U FE mesh 32×16 (C = 87.41); (d) MTOP Q4/n25 (C = 88.01); (e) iMTOP Q4/n25/d4 (C = 88.03); and (f) adaptive Q4/U and Q4/n25/d4 (C = 88.71), (c–f: FE mesh 32×16).

DOI: 10.1002/nme

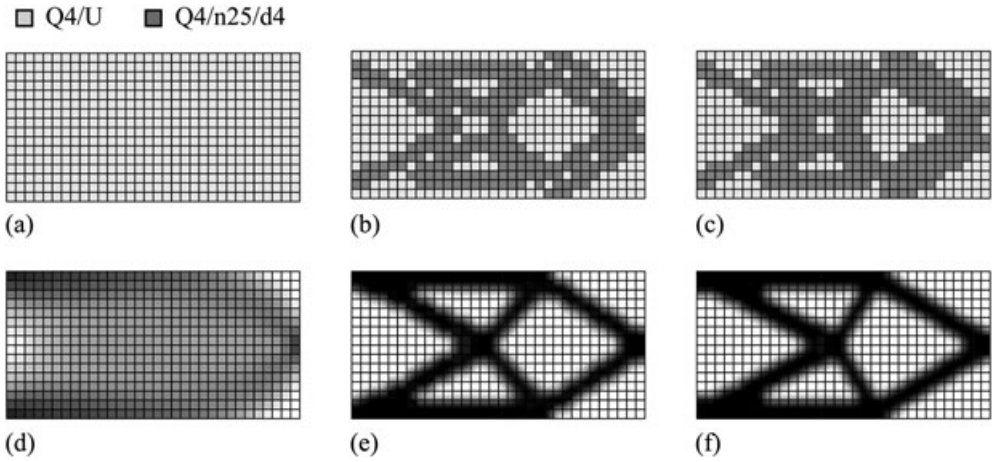

Figure 17. Adaptive topology optimization: (a) initial mesh (512 Q4/U); (b) intermediate mesh (244 Q4/U and 268 Q4/n25/d4); (c) final mesh (222 Q4/U and 290 Q4/n25/d4); and (d-e-f) initial, intermediate and final adaptive topologies, respectively.

and Q4/n25/d4 are used in the adaptive procedure; however, it is noted that more than one iMTOP element type can be employed in the proposed approach.

6. THREE-DIMENSIONAL NUMERICAL EXAMPLES

This section demonstrates the capability of the proposed schemes to handle relatively large-scale three-dimensional applications. First, a cube with a concentrated load at the bottom and a building subjected to a torsion load are presented to demonstrate the iMTOP scheme. Second, a three-dimensional cantilever beam is considered to demonstrate the adaptive procedure. Similarly to Section 5, all the quantities are dimensionless, Young's modulus is chosen as 1, and Poisson's ratio is 0.3.

6.1. A cube with concentrated load at the bottom center

This example investigates a cube that is constrained at four bottom corners in the vertical directions and subjected to a vertical load at the center of the bottom face as shown in Figure 18(a). The cube domain has edge length of $L = 48$. The domain is divided into 24×24×24 B8 elements, which results in a total of 13,824 brick elements. Because of the symmetry condition, only one fourth of the cube is taken into computation. We aim to find the optimal topology with volume fraction constraint of 10%, minimum length scale $L/20$, and penalization parameter $p = 4$.

First, the problem is solved using MTOP B8/n125 elements, which use 125 density elements and 125 design variables per brick element. The optimal topology is shown in Figure 18(b) with iso-surface density of 0.25. Next, we employ the iMTOP approach and reduce the number of design variables by using B8/n125/d64, B8/n125/d27, and B8/n125/d8 elements. The corresponding topologies are shown in Figures 18(c)–(e), respectively. The resolutions of these designs are comparable to the design shown in Figure 18(b) using MTOP B8/n125 elements. Additionally, the values of the compliances of the optimal topologies obtained from MTOP and iMTOP, using the same number of density elements and different number of design variables, are similar as shown in Figure 18.

The convergence histories of optimization process are shown in Figure 19(a). Similarly to the 2D example in Section 5.1, Figure 19(a) shows close convergence history for different iMTOP element types. The computational cost comparison is shown in Figure 19(b). It can be seen that the computational times of B8/n125/d64, B8/n125/d27, and B8/n125/d8 elements are much less than that of the MTOP B8/n125 element. For example, the computational time of B8/n125/d8 element is only

DOI: 10.1002/nme

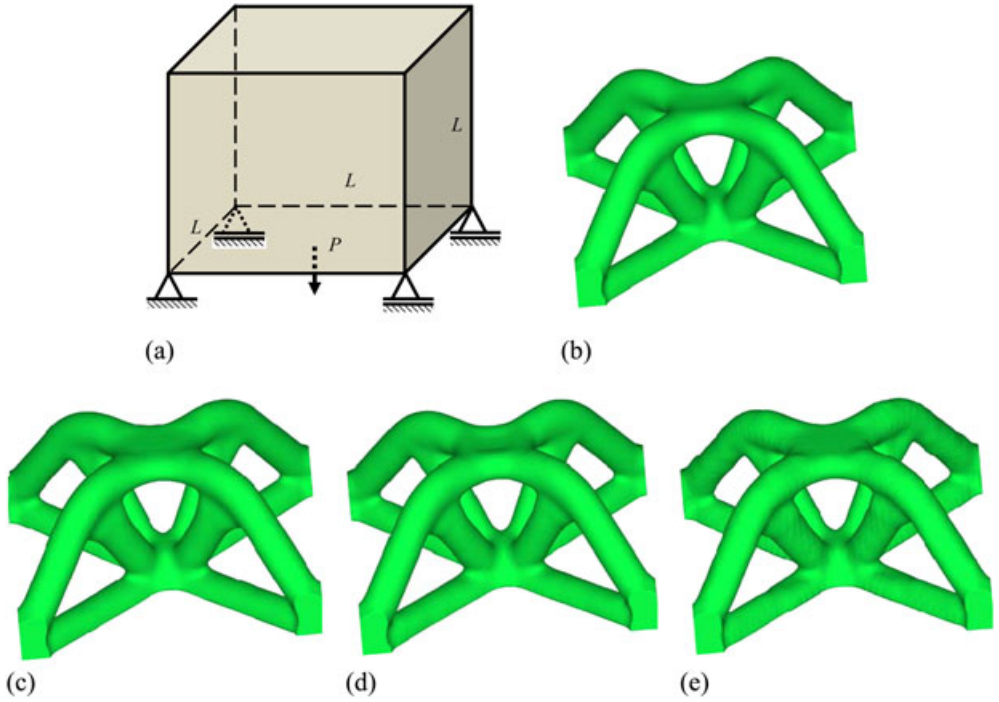

Figure 18. Topology optimization of a cube (FE mesh $24 \times 24 \times 24$): (a) geometry; (b) MTOP B8/n125 (C = 29.04); (c) iMTOP B8/n125/d64 (C = 29.06); (d) iMTOP B8/n125/d27 (C = 29.08); and (e) iMTOP B8/n125/d8 (C = 29.33).

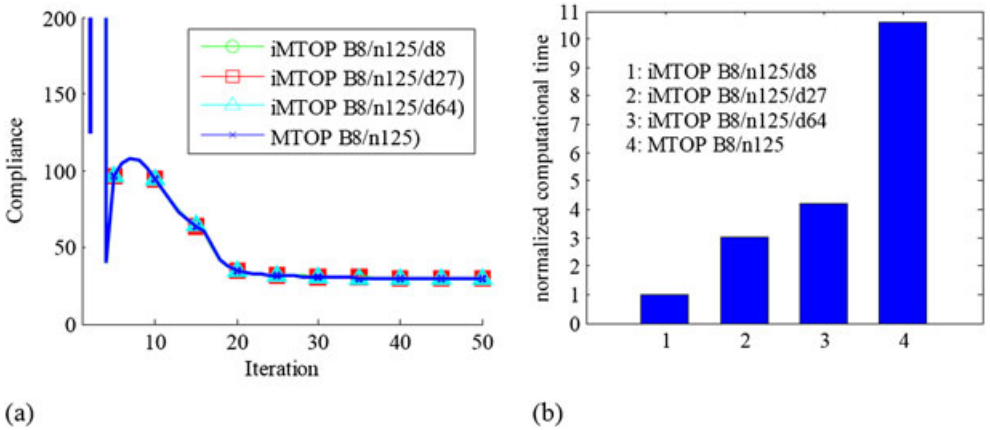

Figure 19. Results of the cube optimization after 50 iterations: (a) convergence history; and (b) computational times.

one tenth of the B8/n125 element. This is because the iMTOP B8/n125/d8 element utilizes about 15 times less design variables than MTOP B8/n125 element.

The computational time can be compared by considering Figure 13(b) (for the MBB example) and Figure 19(b) (for the 3D cube example). The efficiency of these approaches is compared more effectively if we consider the computational data. Table II shows the computational data for the 2D MBB beam example and the 3D cube example. It is seen that the MTOP and iMTOP approaches require less numbers of finite elements and design variables to achieve the same resolution designs by the conventional approach. For instance, in the cube example, to have the same resolution by the MTOP and iMTOP approaches using $n = 125$ density elements per B8, the element-based approach has to utilize 1,728,000 finite elements. By contrast, the MTOP and iMTOP approaches employ only 13,824 finite elements. Moreover, the iMTOP approach can reduce the number of design variables

DOI: 10.1002/nme

Table II. Computational data of the MBB beam and cube examples.

Example	Approaches	Element types	Figure	Number of			iMTOP ratio
				Finite elements	Density elements	Design variables	k:n:d
MBB	Element-based fine mesh	Q4/U	11(a)	30,000	30,000	30,000	25 : 25 : 25
	MTOP	Q4/n25	11(c)	1,200	30,000	30,000	1 : 25 : 25
	iMTOP	Q4/n25/d16	11(d)	1,200	30,000	19,200	1 : 25 : 16
		Q4/n25/d9	11(e)	1,200	30,000	10,800	1 : 25 : 9
		Q4/n25/d4	11(f)	1,200	30,000	4,800	1 : 25 : 4
	Element-based coarse mesh	Q4/U	11(b)	1,200	1,200	1,200	1 : 1 : 1
Cube	Element-based fine mesh	B8/U	N/A	1,728,000	1,728,000	1,728,000	125 : 125 : 125
	MTOP	B8/n125	18(b)	13,824	1,728,000	1,728,000	1 : 125 : 125
	iMTOP	B8/n125/d64	18(c)	13,824	1,728,000	884,736	1 : 125 : 64
		B8/n125/d27	18(d)	13,824	1,728,000	373,248	1 : 125 : 27
		B8/n125/d8	18(e)	13,824	1,728,000	110,592	1 : 125 : 8

N/A, not available.

from 1,728,000 in the MTOP approach (for B8/n125) to only 110,592 (for B8/n125/d8), while maintaining the same resolution. Thus, the computational data (the number of finite elements, density elements and design variables, and the iMTOP ratio) in Table II can serve as an indicator of the efficiency and resolution levels of the topology optimization model.

6.2. A building with torsion loading

This example demonstrates the iMTOP scheme used for optimization the topology of a building under torsion. Figure 20(a) shows the domain with with the dimension of $L \times L \times 4L$. Four unit loads are applied at the middle of the four top edges to create a torsion load. The domain is divided into $10 \times 10 \times 40$ B8 elements, which results in a total of 4,000 brick elements. The volume fraction constraint of 10%, the minimum length scale $r_{\min} = 0.12L$, and penalization parameter $p = 3$ are employed. We utilize different MTOP and iMTOP elements and obtain the topologies as shown in Figure 20. Similarly to the previous example, iMTOP elements using less number of design variables than density elements can provide the resolution comparable to the MTOP elements. Moreover, the arrangement of structural members in Figure 20 is similar to the Michell's type optimal solution for space truss subjected to torsion loading [49].

6.3. Cantilever beam with concentrated load

This example demonstrates the capability of the adaptive procedure (AMTOP) for three-dimensional applications. A three-dimensional cantilever with the domain $2L \times L \times L$ shown in Figure 21(a) is considered. The domain is divided into $24 \times 12 \times 12$ B8 elements, which results in a total of 3,456 brick elements. A volume fraction constraint of 30%, a minimum length scale of one tenth of the beam height $r_{\min} = L/10$, and penalization parameter $p = 3$ are employed. First, the problem is solved using B8/U elements, which provides the results shown in Figure 21(b). Second, the iMTOP approach using B8/n125/d8 leads to the topology shown in Figure 21(c). Finally, the adaptive approach using B8/U and B8/n125/d8 provides the optimal design shown in Figure 21(d).

Table III shows the computational data for the adaptive approach of the cantilever beam for 2D (Section 5.3) and 3D (Section 6.3). It is seen that the use of the adaptive approach can further reduce the numbers of density elements and design variables while maintaining the resolution. In the adaptive approach (AMTOP), the same number of finite elements is considered in the optimization process and the final design has similar resolution as the iMTOP approach. Therefore, the iMTOP ratio in the adaptive approach with lower numbers of density elements (n) and design

DOI: 10.1002/nme

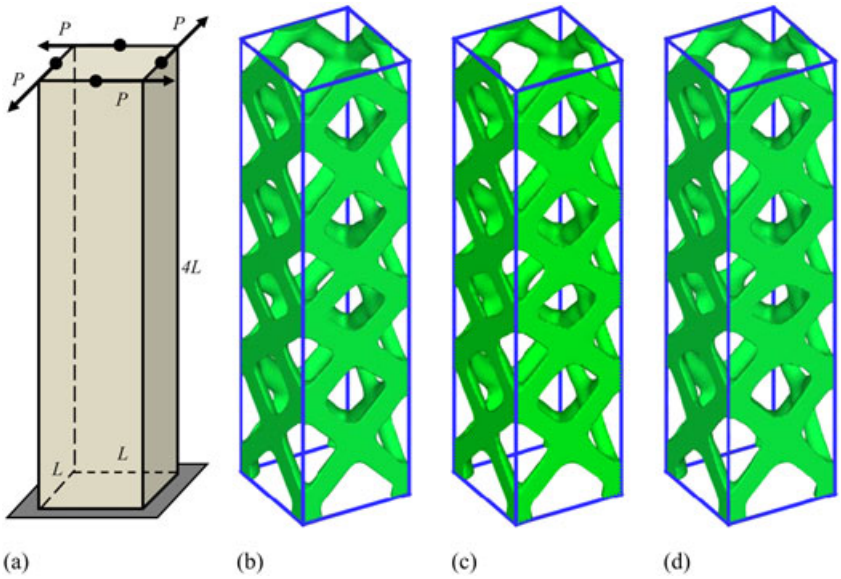

Figure 20. Geometry and optimal topologies of the building under torsion load: (a) geometry; (b) MTOP B8/n125; (c) iMTOP B8/n125/d27; and (d) iMTOP B8/n125/d8.

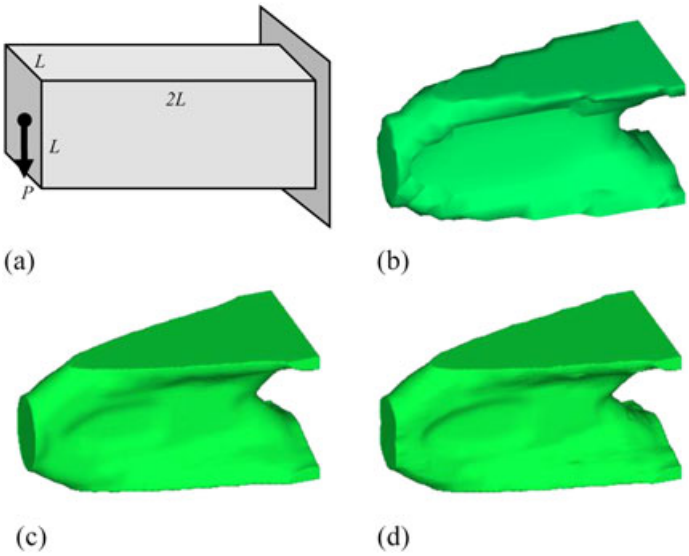

Figure 21. Topologies from element-based, iMTOP, and adaptivity on FE mesh $24 \times 12 \times 12$: (a) geometry of a cantilever beam 3D (2:1:1); (b) element-based B8/U (C = 5.088); (c) iMTOP B8/n125/d8 (C = 5.182); and (d) adaptivity B8/U and B8/n125/d8 (C = 5.283).

variables (d) means a more efficient model in comparison with the iMTOP approach. For example, in the 2D cantilever, the 'iMTOP ratio' is 1 : 1 : 1 for the element-based approach on a coarse mesh. This ratio can be improved to 1 : 25 : 25 for MTOP Q4/n25 elements and 1 : 25 : 4 for iMTOP Q4/n25/d4 elements. The adaptive approach improves the iMTOP ratio from 1 : 1 : 1 to 1 : 14.5 : 2.5 at the final adaptive iteration. Similarly in the 3D case, the iMTOP ratio is changed during the adaptive optimization process. For example, an intermediate iteration (iteration 5) has 2,288 B8/U and 1,168 B8/n125/d8 elements and the final iteration (iteration 100) has 2,072 B8/U and 1,384 B8/n125/d8 elements. The iMTOP ratio is improved from 1 : 1 : 1 to 1 : 50.7 : 3.8 at the final adaptive iteration. This means that lower numbers of density elements and design variables are employed by the adaptive approach in comparison to the iMTOP and the element-based approaches while a design with similar resolution is achieved.

DOI: 10.1002/nme

Table III. Computational data of the 2D and 3D cantilever examples.

Example	Approaches	Element types	Figure	Number of			iMTOP ratio
				Finite elements	Density elements	Design variables	k: n: d
2D cantilever	Element-based fine mesh	Q4/U	16(b)	12,800	12,800	12,800	25 : 25 : 25
	MTOP	Q4/$n25$	16(d)	512	12,800	12,800	1 : 25 : 25
	iMTOP	Q4/$n25/d4$	16(e)	512	12,800	2,048	1 : 25 : 4
	adaptive (initial iteration)	Q4/U	17(a),(d)	512	512	512	1 : 1 : 1
	adaptive (intermediate iteration)	Q4/U and Q4/$n25/d4$	17(b),(e)	512	6,944	1,316	1 : 13.6 : 2.6
	adaptive (final iteration)	Q4/U and Q4/$n25/d4$	17(c),(f)	512	7,472	1,382	1 : 14.6 : 2.7
	Element-based coarse mesh	Q4/U	16(c)	512	512	512	1 : 1 : 1
3D cantilever	Element-based fine mesh	B8/U	N/A	432,000	432,000	432,000	125 : 125 : 125
	iMTOP	B8/$n125/d8$	21(c)	3,456	432,000	27,648	1 : 125 : 8
	adaptive (initial iteration)	B8/U	N/A	3,456	3,456	3,456	1 : 1 : 1
	adaptive (intermediate iteration)	B8/U and B8/$n125/d8$	N/A	3,456	148,288	11,632	1 : 42.9 : 3.4
	adaptive (final iteration)	B8/U and B8/$n125/d8$	21(d)	3,456	175,072	13,144	1 : 50.7 : 3.8
	Element-based coarse mesh	B8/U	21(b)	3,456	3,456	3,456	1 : 1 : 1

DOI: 10.1002/nme

7. CONCLUSIONS

In this study, we proposed a computational paradigm for improving multiresolution topology (iMTOP) via three distinct meshes (not necessarily uncorrelated): the finite element mesh, design variable mesh, and the density mesh. By using a relatively coarse mesh for analysis, a moderately fine mesh for design variables, and a relatively fine mesh for density elements, we can obtain high fidelity designs with a relatively low computational cost. A projection scheme is introduced to compute element densities from design variables and to control the length scale of the density. Furthermore, we propose a heuristic adaptive multiresolution topology optimization (AMTOP) procedure to further reduce the computational cost by using iMTOP elements only where and when needed. Therefore, the number of density elements and the number of design variables are potentially less than the original iMTOP approach. The proposed techniques and their merits were demonstrated by various two-dimensional and three-dimensional numerical examples.

This study has shown the features of the iMTOP and AMTOP approaches to obtain high resolution design over the conventional topology optimization approach. Future studies can further explore the optimal number and locations of the design variables. Future topics for further investigation also include the applications of the iMTOP and AMTOP approaches to multiphysics and multiscale problems [50, 51], stress constraint problems [52], energy harvesting devices [53], reliability-based design and topology optimization problems [22, 54], and dynamics problems [55].

NOMENCLATURE

$\mathbf{d}$	= vector of design variables
C	= compliance
V_s	= prescribed volume
V	= volume
$\mathbf{x}$	= position of a point in the domain, coordinate vector
$volfrac$	= volume fraction
$N_i(.)$	= shape function
$\mathbf{D}^0$	= constitutive matrix corresponding to the solid material
$\mathbf{D}$	= constitutive matrix
$\mathbf{B}$	= strain–displacement matrix consisting of shape function derivatives
$\mathbf{K}$	= global stiffness matrix
$\mathbf{K}_e$	= stiffness matrix of displacement element e
$\mathbf{K}_e^0$	= stiffness matrix of element e corresponding to the solid material
n	= number of density elements per displacement element
E	= Young's modulus
E^0	= Young's modulus corresponding to solid material
ρ_i	= density of element i
d_n	= design variable n
$r_{\min}$	= minimum length scale
p	= penalization parameter
$f(.)$	= projection function
$\mathbf{u}$	= global displacement vector
$\mathbf{f}$	= global load vector
A_i	= area (or volume) of the density element i in the initial domain
A_i^0	= area (or volume) of the density element i in the reference domain
$w(.)$	= weight function in the projection scheme
Q4/$n25$	= MTOP Q4 element with 25 density elements and 25 design variables
Q4/$n25$/$d4$	= iMTOP Q4 element with 25 density elements and 4 design variables
B8/$n125$	= MTOP B8 element with 125 density elements and 125 design variables
B8/$n125$/$d8$	= iMTOP B8 element with 125 density elements and 8 design variables

DOI: 10.1002/nme

ACKNOWLEDGEMENTS

This research was funded in part by a grant from the Vietnam Education Foundation (VEF) and by the National Science Foundation (NSF). GHP's contribution was based on work supported by the National Science Foundation, while working at the foundation as a program director. Any opinion, finding, conclusions, or recommendations expressed in this material are those of the authors and do not necessarily reflect the views of the sponsors.

REFERENCES

1. Suzuki K, Kikuchi N. A homogenization method for shape and topology optimization. *Computer Methods in Applied Mechanics and Engineering* 1991; **93**(3):291–318.
2. Rozvany GIN. Aims, scope, methods, history and unified terminology of computer-aided topology optimization in structural mechanics. *Structural and Multidisciplinary Optimization* 2001; **21**(2):90–108.
3. Bendsøe MP. Optimal shape design as a material distribution problem. *Structural and Multidisciplinary Optimization* 1989; **1**(4):193–202.
4. Wang S, de Sturler E, Paulino GH. Large-scale topology optimization using preconditioned Krylov subspace methods with recycling. *International Journal for Numerical Methods in Engineering* 2007; **69**(12):2441–2468.
5. Borrvall T, Petersson J. Large-scale topology optimization in 3D using parallel computing. *Computer Methods in Applied Mechanics and Engineering* 2001; **190**(46-47):6201–6229.
6. Evgrafov A, Rupp CJ, Maute K, Dunn ML. Large-scale parallel topology optimization using a dual-primal substructuring solver. *Structural and Multidisciplinary Optimization* 2008; **36**(4):329–345.
7. Mahdavi A, Balaji R, Frecker M, Mockensturm EM. Topology optimization of 2D continua for minimum compliance using parallel computing. *Structural and Multidisciplinary Optimization* 2006; **32**(2):121–132.
8. Kim TS, Kim JE, Kim YY. Parallelized structural topology optimization for eigenvalue problems. *International Journal of Solids and Structures* 2004; **41**(9-10):2623–2641.
9. Amir O, Stolpe M, Sigmund O. Efficient use of iterative solvers in nested topology optimization. *Structural and Multidisciplinary Optimization* 2010; **42**(1):55–72.
10. Amir O, Bendsoe MP, Sigmund O. Approximate reanalysis in topology optimization. *International Journal for Numerical Methods in Engineering* 2009; **78**(12):1474–1491.
11. Lin CY, Chou JN. A two-stage approach for structural topology optimization. *Advances in Engineering Software* 1999; **30**(4):261–271.
12. Kim IY, Kwak BM. Design space optimization using a numerical design continuation method. *International Journal for Numerical Methods in Engineering* 2002; **53**(8):1979–2002.
13. Jang IG, Kwak BM. Evolutionary topology optimization using design space adjustment based on fixed grid. *International Journal for Numerical Methods in Engineering* 2006; **66**(11):1817–1840.
14. Guest JK, Prévost JH, Belytschko T. Achieving minimum length scale in topology optimization using nodal design variables and projection functions. *International Journal for Numerical Methods in Engineering* 2004; **61**(2):238–254.
15. Rahmatalla SF, Swan CC. A Q4/Q4 continuum structural topology optimization implementation. *Structural and Multidisciplinary Optimization* 2004; **27**(1):130–135.
16. Matsui K, Terada K. Continuous approximation of material distribution for topology optimization. *International Journal for Numerical Methods in Engineering* 2004; **59**(14):1925–1944.
17. Paulino GH, Le CH. A modified Q4/Q4 element for topology optimization. *Structural and Multidisciplinary Optimization* 2009; **37**(3):255–264.
18. de Ruiter MJ, van Keulen F. Topology optimization using a topology description function. *Structural and Multidisciplinary Optimization* 2004; **26**(6):406–416.
19. Paulino GH, Pereira A, Talischi C, Menezes IFM, Celes W. Embedding of superelements for three-dimensional topology optimization. In *Proceedings of Iberian Latin American Congress on Computational Methods in Engineering (CILAMCE)*, Macieo, Brazil, 2008.
20. Nguyen TH, Paulino GH, Song J, Le CH. A computational paradigm for multiresolution topology optimization (MTOP). *Structural and Multidisciplinary Optimization* 2010; **41**(4):525–539.
21. Sutradhar A, Paulino GH, Miller MJ, Nguyen TH. Topological optimization for designing patient-specific large craniofacial segmental bone replacements. *Proceedings of the National Academy of Sciences* 2010; **107**(30):13222–13227.
22. Nguyen TH, Song J, Paulino GH. Single-loop system reliability-based topology optimization considering statistical dependence between limit states. *Structural and Multidisciplinary Optimization* 2011; **44**(5):593-611.
23. Nguyen TH, Song J, Paulino GH. Challenges and advances in system reliability based optimization of structural topology. In *Proceedings of the 19th Analysis and Computation Specialty Conference*, Orlando, Florida, U.S.A., 2010; 480–491.
24. Costa Jr JCA, Alves MK. Layout optimization with h-adaptivity of structures. *International Journal for Numerical Methods in Engineering* 2003; **58**(1):83–102.
25. Stainko R. An adaptive multilevel approach to the minimal compliance problem in topology optimization. *Communications in Numerical Methods in Engineering* 2006; **22**(2):109–118.

DOI: 10.1002/nme

26. de Sturler E, Paulino GH, Wang S. Topology optimization with adaptive mesh refinement. In *Proceedings of the 6th International Conference on Computation of Shell and Spatial Structures IASS-IACM 2008: 'Spanning Nano to Mega'*, Ithaca, NewYork, U.S.A., 2008.
27. Maute K, Ramm E. Adaptive topology optimization. *Structural and Multidisciplinary Optimization* 1995; **10**(2):100–112.
28. Kim YY, Yoon GH. Multi-resolution multi-scale topology optimization—a new paradigm. *International Journal of Solids and Structures* 2000; **37**(39):5529–5559.
29. Kim JE, Jang GW, Kim YY. Adaptive multiscale wavelet-Galerkin analysis for plane elasticity problems and its applications to multiscale topology design optimization. *International Journal of Solids and Structures* 2003; **40**(23):6473–6496.
30. Guest JK, Genut LCS. Reducing dimensionality in topology optimization using adaptive design variable fields. *International Journal for Numerical Methods in Engineering* 2009; **81**(8):1019–1045.
31. Talischi C, Paulino GH, Pereira A, Menezes IFM, Celes W. Polygonal finite elements for topology optimization: a unifying paradigm. *International Journal for Numerical Methods in Engineering* 2010; **82**(6):671–698.
32. Nguyen TH. System reliability-based design and multiresolution topology optimization. *Ph.D Thesis*, Department of Civil and Environmental Engineering, University of Illinois at Urbana-Champaign, 2010.
33. Poulsen TA. Topology optimization in wavelet space. *International Journal for Numerical Methods in Engineering* 2002; **53**(3):567–582.
34. Diaz A, Sigmund O. Checkerboard patterns in layout optimization. *Structural and Multidisciplinary Optimization* 1995; **10**(1):40–45.
35. Poulsen TA. A simple scheme to prevent checkerboard patterns and one-node connected hinges in topology optimization. *Structural and Multidisciplinary Optimization* 2002; **24**(5):396–399.
36. Sigmund O, Petersson J. Numerical instabilities in topology optimization: a survey on procedures dealing with checkerboards, mesh-dependencies and local minima. *Structural and Multidisciplinary Optimization* 1998; **16**(1):68–75.
37. Sigmund O. On the design of compliant mechanisms using topology optimization. *Mechanics Based Design of Structures and Machines* 1997; **25**(4):493–524.
38. Bruns TE, Tortorelli DA. Topology optimization of non-linear elastic structures and compliant mechanisms. *Computer Methods in Applied Mechanics and Engineering* 2001; **190**(26-27):3443–3459.
39. Bourdin B. Filters in topology optimization. *International Journal for Numerical Methods in Engineering* 2001; **50**(9):2143–2158.
40. Sigmund O. Morphology-based black and white filters for topology optimization. *Structural and Multidisciplinary Optimization* 2007; **33**(4):401–424.
41. Almeida SRM, Paulino GH, Silva ECN. A simple and effective inverse projection scheme for void distribution control in topology optimization. *Structural and Multidisciplinary Optimization* 2009; **39**(4):359–371.
42. Bendsøe MP, Sigmund O. *Topology Optimization: Theory, Methods, and Applications*. Springer: Berlin, 2003.
43. Bendsøe MP, Sigmund O. Material interpolation schemes in topology optimization. *Archive of Applied Mechanics* 1999; **69**(9):635–654.
44. Rozvany GIN, Zhou M, Birker T. Generalized shape optimization without homogenization. *Structural and Multidisciplinary Optimization* 1992; **4**(3):250–252.
45. Cook RD, Malkus DS, Plesha ME, Witt RJ. *Concepts and Applications of Finite Element Analysis*. John Wiley & Sons: New York, 2002.
46. Frecker M, Kikuchi N, Kota S. Topology optimization of compliant mechanisms with multiple outputs. *Structural and Multidisciplinary Optimization* 1999; **17**(4):269–278.
47. Ainsworth M, Oden JT. *A Posteriori Error Estimation in Finite Element Analysis*. Wiley and Sons: New York, 2000.
48. Svanberg K. The method of moving asymptotes- a new method for structural optimization. *International Journal for Numerical Methods in Engineering* 1987; **24**(2):359–373.
49. Rozvany GIN. Some shortcomings in Michell's truss theory. *Structural and Multidisciplinary Optimization* 1996; **12**(4):244–250.
50. Carbonari RC, Silva ECN, Paulino GH. Multi-actuated functionally graded piezoelectric micro-tools design: a multiphysics topology optimization approach. *International Journal for Numerical Methods in Engineering* 2009; **77**(3):301–336.
51. Sigmund O. Design of multiphysics actuators using topology optimization-Part I: One-material structures. *Computer Methods in Applied Mechanics and Engineering* 2001; **190**(49-50):6577–6604.
52. Duysinx P, Bendsøe MP. Topology optimization of continuum structures with local stress constraints. *International Journal for Numerical Methods in Engineering* 1998; **43**(8):1453–1478.
53. Rupp CJ, Evgrafov A, Maute K, Dunn ML. Design of piezoelectric energy harvesting systems: a topology optimization approach based on multilayer plates and shells. *Journal of Intelligent Material Systems and Structures* 2009; **20**(16):1923–1939.
54. Nguyen TH, Song J, Paulino GH. Single-loop system reliability-based design optimization using matrix-based system reliability method: theory and applications. *ASME Journal of Mechanical Design* 2010; **132**(1). 011005-1-11.
55. Bogomolny M. Topology optimization for free vibrations using combined approximations. *International Journal for Numerical Methods in Engineering* 2010; **82**(5):617–636.

DOI: 10.1002/nme